

Learning Constrained Dynamic Correlations in Spatiotemporal Graphs for Motion Prediction

Jiajun Fu , Fuxing Yang , Xiaoli Liu , and Jianqin Yin* 

Abstract—Human motion prediction is a challenging task due to the dynamic spatiotemporal correlations in different motion sequences. How to efficiently represent spatiotemporal correlations and model dynamic correlation variances between different motion sequences is a challenge for spatiotemporal representation in motion prediction. In this work, we propose Dynamic SpatioTemporal Decompose Graph Convolution (DSTD-GC), which decomposes dynamic spatiotemporal graph modeling with a combination of Dynamic Spatial Graph Convolution (DS-GC) and Dynamic Temporal Graph Convolution (DT-GC). The dynamic spatial/temporal correlations in DS-GC/DT-GC are efficiently represented by Constrained Dynamic Correlation Modeling, which is inspired by the common constraints in human motion like body connections and dynamic patterns from different samples. The Constrained Dynamic Correlation Modeling represents the spatial/temporal graph as a combination of a shared spatial/temporal correlation and an unshared correlation extraction function. This spatiotemporal representation is of square space complexity and only requires 28.6% parameters of the state-of-the-art sample-shared decomposition representation. It also explicitly models sample-specific spatiotemporal correlation variances. Moreover, we also mathematically reformulate graph convolutions on spatiotemporal graphs into a unified form and find that DSTD-GC relaxes certain constraints of other graph convolutions, which leads to a stronger representation capability. Combining DSTD-GC with prior knowledge like body connection and temporal context, we propose a powerful spatiotemporal graph convolution network called DSTD-GCN. On the Human3.6M and CMU Mocap datasets, DSTD-GCN outperforms state-of-the-art methods by 3.9% - 5.7% in prediction accuracy with 55.0% - 96.9% parameter reduction.

Index Terms—human motion prediction, spatiotemporal graph convolution, spatiotemporal decomposition, dynamic correlation modeling

I. INTRODUCTION

HUMAN motion prediction is a challenging task that involves modeling dynamic spatiotemporal correlations between body joints. This task is becoming increasingly important in autonomous driving [1], human-machine interaction [2], [3], and healthcare [4].

Traditional methods can handle simple and periodic scenarios with classical time series processing approaches [5], [6], but make unrealistic predictions when the human motion becomes more complex and erratic. Recently, researchers have adopted different deep learning techniques to human motion prediction, such as Convolution Neural Network (CNN) [7], [8], Recurrent Neural Network (RNN) [7], [9]–[11], [11]–[17], Generative Adversarial Network (GAN) [18]–[22] and

Transformer [23], [24]. While these methods have achieved significant advancements over traditional approaches, they are unable to explicitly represent body connections and rely on manual filter size selection [25]. As a human motion sequence is naturally represented as a spatiotemporal graph and can be decomposed into a combination of spatial graphs and temporal graphs (see Figure 1 (a)), Graph Convolutions Network (GCN) have been applied by many researchers in motion prediction [25]–[31]. Earlier GCN-based methods utilized graph convolutions GCs to model shared spatial correlations between joints [25], [26], [28]–[30]. Sofianos et al. [31] first introduced a GC with unshared spatial and temporal correlations, which outperforms correlation-shared GCNs with far fewer parameters.

Despite the promising results of GCN-based models, there are two challenges for realizing high predictability of human motions: (1) *Lightweight spatiotemporal correlation representation*: Although Sofianos et al. [31] directly parameterized the spatiotemporal correlations as unshared spatial and temporal adjacency matrices, this method still introduce redundant parameters to represent shared prior knowledge like body connections and temporal context. There is still room to explore more parameter-saving decomposition representations of spatiotemporal graph. (2) *Sample-specific spatiotemporal correlations*: as shown in Figure 1 (b), spatiotemporal correlations are dynamic and vary between input samples. Graph correlations in all previous works [25]–[31] adopt sample-shared graph correlations. Although the sample-shared correlations are learned through back-propagation and optimal for all data, they may disturb individual prediction by mistakenly enhancing unrelated correlations or reducing critical connection strengths. This leads to amplification of slight movement or the inability to infer future motion from tiny cues.

To handle the aforementioned challenges, we look into *constrained dynamic nature of spatiotemporal correlations*, a key characteristic which all previous GCN-based methods ignore. On the one hand, the spatiotemporal correlations are subject to shared constraints like joint connections and temporal context. On the other hand, the correlation strength between certain joints is dynamically enhanced or reduced according to different samples.

Inspired by this, we introduce Dynamic SpatioTemporal Decompose Graph Convolutions (DSTD-GC), which contains Dynamic Spatial Graph Convolution (DS-GC) and Dynamic Temporal Graph Convolution (DT-GC) for constrained dynamic spatial and temporal correlation modeling. Within the constrained correlation modeling, the shared constrained correlation is parameterized as a vanilla spatial/temporal adjacency matrix, which is shared by all time/joints and all samples. This

* Jianqin Yin is the corresponding author

Jiajun Fu, Fuxing Yang, Xiaoli Liu, and Jianqin Yin are with the School of Artificial Intelligence, Beijing University of Posts and Telecommunications, Beijing, China.

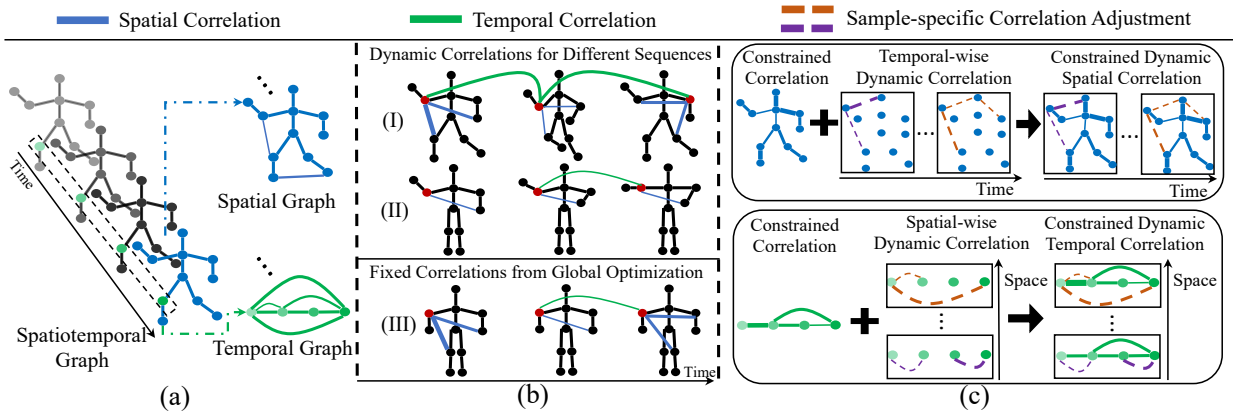


Fig. 1. (a) Spatiotemporal graph representation and decomposition. A spatiotemporal graph can be decomposed into multiple spatial graphs and temporal graphs. (b) Dynamic correlation modeling. Correlations vary from different actions, the correlations in walking (I) are different from the ones in directing traffic (II). The learned correlations from global optimization (III) can't explicitly capture these variations and introduce correlation amplification or reduction. (c) Constrained dynamic correlation modeling. The spatial correlations consist of a shared constrained correlation and an unshared temporal-wise dynamic correlation. Temporal graph correlations contain shared constrained correlations and unshared spatial-wise adjustments. For (b) and (c), the line thickness indicate the correlation strength.

shared correlation serves as motion prior and indicates general connections between vertices. On the other hand, the dynamic refinements are extracted by an adjustment function according to different samples. The sample-specific temporal/spatial-wise adjustments complete sample-shared temporal/spatial-shared constraints. With this formulation, we manage to represent unshared spatial/temporal correlations in quarter space complexity, while the previous representation [31] is of cubic space complexity. Besides, DSTD-GC captures dynamic motion patterns between different samples and adjust correlations between joints, which precisely enhances correlations for mutual movement and reduce correlations for unrelated motion. Furthermore, we analyze different kinds of spatiotemporal graph convolutions in a unified form and theoretically prove that DSTD-GC enhances feature representation by relaxing certain restrictions of spatiotemporal graph convolutions. Combing DSTD-GC and prior knowledge like body connections and temporal context, we propose DCTD-GCN which consistently outperforms other state-of-the-art methods in prediction accuracy with the fewest parameters.

In brief, our contributions are summarized as follow:

- We propose Dynamic SpatioTemporal Decompose Graph Convolution, which utilizes Constrained Dynamic Correlation Modeling to represent sample-specific unshared correlations in spatiotemporal graph, leading to effective spatiotemporal correlation representation and accurate motion prediction.
- We mathematically unify all forms of graph convolutions in human motion prediction and show that DSTD-GCN improves representative ability by relaxing limitations of other graph convolutions.
- We show with extensive experiments that our proposed DSTD-GCN outperforms other state-of-the-art methods in terms of prediction errors and parameter numbers on two benchmark datasets.

II. RELATED WORK

A. Human Motion Prediction

Researchers have applied various deep learning techniques in human motion prediction. CNN-based methods mainly treat a human pose as a pseudo-image. [7], [8]. Liu *et al.* [8] stacked pose sequence along the channel dimension and extract multi-level motion features in different CNN layers. RNN-based methods shows their power in modeling temporal motion features and make consistent predictions [7], [11]–[17], [28], [30], [32]. Martinez *et al.* proposed a simple yet efficient Seq2Seq model and make prediction based on residual velocities. Wang *et al.* [17] extends this framework by introducing joint velocity and frame position. GAN-based methods make multiple future predictions based on data pattern similarities and generate realistic results [18], [29], [33], [34]. Lyu *et al.* [34] utilized stochastic differential equations and path integrals. Transformer-based methods directly model long-range spatial and temporal dependencies [23], [24]. Aksan *et al.* designed spatial and temporal transformer to simultaneously update spatiotemporal representation. Although these methods make remarkable advancements compared with traditional methods, they can't directly model natural connectivity between body joints. The natural connectivity is crucial for human motion prediction as human motion follows kinetic chains and trajectory path, which are constrained by body connections and temporal context, respectively. In order to explicitly model body connections, researchers have looked into graph convolution networks (GCNs). Graph Convolutions (GCs) are suitable for non-grid and graph-structural data, which has been successfully applied to social network [35], point cloud [36] and traffic prediction [37]. With joints as vertices, bone and trajectory connections as edges, a human pose can be naturally represented as a spatiotemporal graph. Recently, many researchers has applied GCs in motion prediction [25]–[27], [29]–[31], [38].

B. Graph Convolution Networks in Motion Prediction

Nearly all GCN-based prediction approaches were developed based on Kipt et al. [39], where features are updated in a two-step manner: (1) Feature transformation with a simple linear transformation or a multi-layer perceptron; and (2) Feature aggregation with graph correlations. The graph correlation is the key component that set GCN apart from other deep learning techniques, which explicitly depicts body connections flexibly. For the spatiotemporal graph correlation, all human prediction methods decomposed it into spatial correlations and temporal correlations. Based on decomposed graph correlations, there are two classifications: (1) *Correlation-shared/Correlation-unshared*: this is according to whether graph correlations are shared by joints in temporal-wise spatial graphs or spatial-wise temporal graphs. (2) *Sample-shared/Sample-specific*: this is based on whether graph correlations are adjusted dynamically to different samples.

1) *Correlation-shared/Correlation-unshared Methods*: For correlation-shared methods, the spatial/temporal correlations are shared across time/joints. Most of previous works [25]–[27], [29], [30], [38] belong to this type. A challenge for these methods is that they can't explicitly model changing spatial relationships in different stages of the motion and diverse temporal patterns in different joints. Thus, they generally need to stack many GC layers to model complex spatiotemporal correlations in human motion. For *correlation-unshared methods*, the spatial correlations vary from time and the temporal correlations vary from joints. Thus, these methods can explicitly depict joint relationships in spatiotemporal graphs and thus explicitly model complex spatiotemporal correlations in human motion with far fewer parameters [31].

2) *Sample-shared/Sample-specific Methods*: For sample-shared methods, graph correlations keep unchanged for all samples. Nearly all previous works applied this strategy. Mao et al. [26] and Dang et al. [25] directly learned graph correlations from data, while Li et al. [28] initialize the trainable correlation as a predefined graph. Cui et al. [29] and Liu et al. [30] combined previous two correlations and proposed a semi-constrained graph correlation. For *sample-specific methods*, graph correlations can be adjusted to each sample. To our best knowledge, sample-specific GCs are hardly studied in motion prediction. We are the first work to model *sample-specific correlation-unshared GC* in motion prediction.

III. METHODOLOGY

A. Preliminaries

1) *Problem Definition*: Human motion prediction is to predict L future human pose frames with K historical observations. As a human pose is represented by J joints with D -dimensional spatial information, we denote the human pose at time t as $X_t \in \mathbb{R}^{J \times D}$. The historical observations are formulated as $X_{1:K} = \{X_1, \dots, X_K\}$. Our goal is to predict the future human motion $\tilde{X}_{K+1:K+L} = \{\tilde{X}_{K+1}, \dots, \tilde{X}_{K+L}\}$ where the corresponding ground truth is denoted as $X_{K+1:K+L} = \{X_{K+1}, \dots, X_{K+L}\}$.

2) *Notations*: We formally define spatiotemporal graph and its decomposition used in this paper.

Spatiotemporal Graph Representation. As shown in Figure 1 (a), a human motion sequence with T frames is presented as a spatiotemporal graph $\mathcal{G}^{st} = (\mathcal{V}^{st}, \mathcal{E}^{st})$, where $\mathcal{V}^{st} \in \mathbb{R}^{JT}$ is the set of all joints across time and \mathcal{E}^{st} is the spatiotemporal edge set. $\mathbf{A}^{st} \in \mathbb{R}^{JT \times JT}$ is the spatiotemporal adjacency matrix, which represent correlations between vertices in the graph. However, it cost a lot of parameters to directly store and learn spatiotemporal correlations with $O((JT)^2)$ space complexity. Therefore, we further decompose a spatiotemporal graph into a unique pair of T spatial graphs across time and J temporal graphs across joints. The spatial graphs are denoted as $\mathcal{G}^s = (\mathcal{V}^s, \mathcal{E}^s)$ where $\mathcal{V}^s \in \mathbb{R}^{T \times J}$ is the joint vertex set. \mathcal{E}^s is the spatial edge set and is formulated as a temporal-unshared spatial adjacency matrix¹ $\mathbf{A}^s \in \mathbb{R}^{T \times J \times J}$. When spatial correlations are shared across time, the spatial adjacency matrix is degraded into vanilla form and is represented by a matrix from $\mathbb{R}^{J \times J}$. Similarly, the temporal graphs are denoted as $\mathcal{G}^t = (\mathcal{V}^t, \mathcal{E}^t)$ where $\mathcal{V}^t \in \mathbb{R}^{J \times T}$ is the trajectory vertex set. \mathcal{E}^t is the temporal edge set and is formulated as a spatial-unshared temporal adjacency matrix $\mathbf{A}^t \in \mathbb{R}^{J \times T \times T}$.

Spatiotemporal-equivalence. Spatiotemporal-equivalence is defined between two functions on spatial graphs and corresponding temporal graphs. Formally, function \mathcal{F}^s on \mathcal{G}^s and function \mathcal{F}^t on corresponding \mathcal{G}^t are spatiotemporal-equivalent if and only if \mathcal{F}^s is equivalent to \mathcal{F}^t after switching all operations for time and space dimension and vice versa. GCs with spatiotemporal-equivalent operations are called spatiotemporal-equivalent GC.

3) *Spatiotemporal Decompose Graph Convolutions*: We introduce different GCs with the example of the feature updating process for the joint q of time n . The neighbor indices of the selected joint in the spatial graph and the temporal graph are p and m , respectively. For a typical spatiotemporal graph convolution (ST-GC), the output feature \mathbf{y}_{qn} is obtained by:

$$\mathbf{y}_{qn} = \sum_p \sum_m a_{(pm)(qn)}^{st} \mathbf{x}_{pm} \mathbf{W}, \quad (1)$$

where $\mathbf{x}_{pm} \in \mathbb{R}^C$ is the input feature, $\mathbf{y}_{qn} \in \mathbb{R}^{C'}$ is the output feature, $a_{(pm)(qn)}^{st}$ is a correlation strength in the spatiotemporal adjacency matrix \mathbf{A}^{st} and $\mathbf{W} \in \mathbb{R}^{C \times C'}$ is a trainable parameter for feature transformation.

With the graph decomposition introduced above, we define two graph GCs: spatial graph convolution (S-GC) and temporal graph convolution (T-GC), which are described as:

$$\mathbf{x}_{qn}^s = \sum_p a_{npq}^s \mathbf{x}_{pn} \mathbf{W}, \quad (2)$$

$$\mathbf{x}_{qn}^t = \sum_m a_{qmn}^t \mathbf{x}_{qm} \mathbf{W}. \quad (3)$$

Specifically, the S-GC models temporal-wise spatial correlations, while T-GC models spatial-wise temporal correlations.

¹We denote both second and third order tensor as matrix in this paper for clarity.

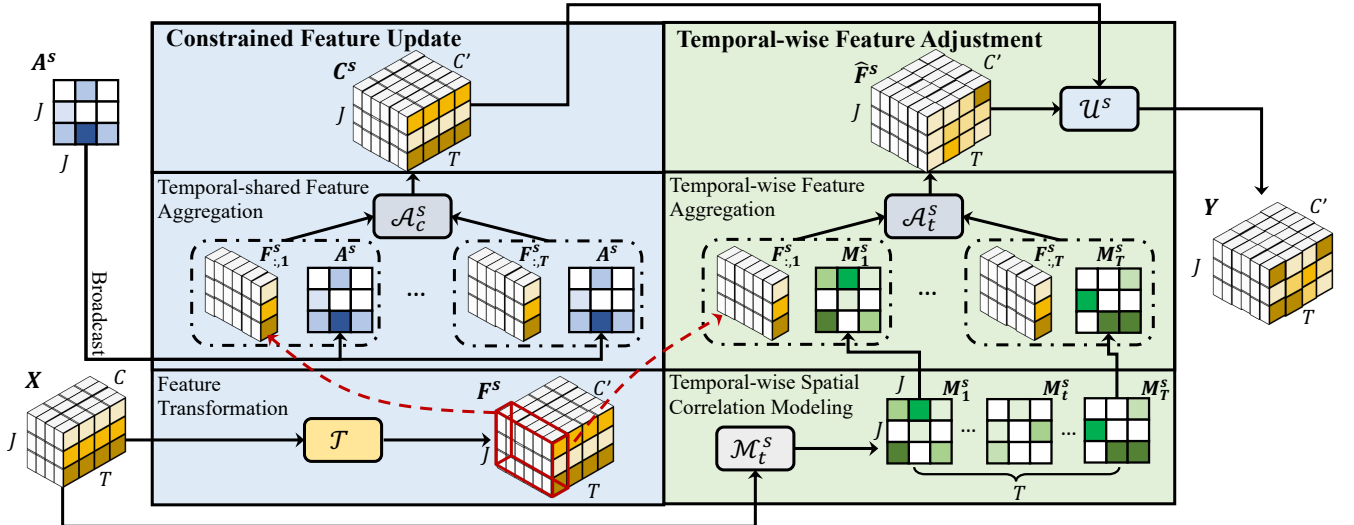


Fig. 2. The framework of Dynamic Spatial Graph Convolution. Constrained feature update aggregates motion representation with temporal-shared correlations. Temporal-wise Feature Adjustment obtains motion representations with temporal-specific correlations, where the correlations are obtained with temporal-wise correlation modeling. Eventually, the output feature is obtained by constrained correlations with temporal-wise adjustment. The introduction of DT-GC is omitted due the spatiotemporal-equivalence between DS-GC and DT-GC.

We then propose *SpatioTemporal Decompose Graph Convolution (STD-GC)* by alternatively stacking a S-GC (Equation 2) and a T-GC (Equation 3):

$$\mathbf{y}_{qn} = \sum_m^T a_{qmn}^t \left(\sum_p^J a_{npq}^s \mathbf{x}_{pm} \mathbf{W}_1 \right) \mathbf{W}_2, \quad (4)$$

where a_{npq}^s and a_{qmn}^t are from spatial adjacency matrix \mathbf{A}^s and temporal adjacency matrix \mathbf{A}^t . STD-GC decomposes ST-GC on a spatiotemporal graph into S-GC on spatial graphs and T-GC on temporal graphs, spatiotemporal feature modeling is accomplished by stacking these two GCs. The spatiotemporal modeling capability is invariant to the stacking order of S-GC and T-GC. Besides, STD-GC is equivalent to STS-GC [31]. We demonstrate all of these with experiments in Section IV-C. Furthermore, STD-GC becomes vanilla STD-GC (VSTD-GC) when the spatial and temporal correlations are in vanilla form.

In sample-shared methods, a_{npq}^s and a_{qmn}^t are set based on prior knowledge or defined as trainable parameters. In sample-specific methods, a_{npq}^s and a_{qmn}^t are generated by model according to input samples.

B. Constrained Dynamic Correlation Modeling

The correlations between joints are both constrained and dynamic. For one thing, the correlations between joints are constrained by the inherent human body structure and learned motion prior. For another, these constrained correlations are varied from different motion sequences. To show these two aspects, we utilize correlations of the elbow joint in the walking and directing traffic scenarios as an example. On the one hand, the elbow movement generally follows the motion chain of the human body and shared trajectory patterns. These constraints are represented by shared spatiotemporal correlations. On the other hand, the spatial correlations between the elbow joint and the knee joint are generally stronger than the correlation

in directing traffic scenarios, and temporal correlations in the knee joint are stronger than the ones in directing traffic.

Inspired by this, we can represent spatiotemporal graph correlations with lightweight vanilla spatial and temporal adjacency matrices and a function to extract dynamic unshared correlations. Therefore, we introduce *Dynamic SpatioTemporal Decompose Graph Convolution (DSTD-GC)*. DSTD-GC extends STD-GC with Dynamic Spatial Graph Convolution and Dynamic Temporal Graph Convolution. Specifically, DS-GC update motion feature with constrained dynamic spatial correlations, while DT-GC with constrained dynamic temporal correlations. By combing these two GCs, DSTD-GC can model constrained dynamic spatiotemporal correlations. These two GCs are spatialtemporal-equivalent. For clarity, We only introduce DS-GC, and its spatiotemporal-equivalent counterpart DT-GC can be deduced naturally. The general framework of DS-GC is illustrated in Figure 2. Specifically, DS-GC consists of two parts: (1) Constrained feature update with shared vanilla correlations; (2) Temporal-wise feature adjustment. The first part updates motion features with shared constraints, while the last part completes feature representations by modeling sample-specific temporal-wise spatial correlation adjustments. Specifically, A DS-GC layer receives motion feature $\mathbf{X} \in \mathbb{R}^{J \times T \times C}$ and shared constrained spatial correlation $\mathbf{A}^s \in \mathbb{R}^{J \times J}$ as inputs, and then outputs $\mathbf{Y} \in \mathbb{R}^{J \times T \times C}$.

1) *Constrained Feature Update*: As shown in the blue block of Figure 2, constrained feature update is identical to vanilla S-GC where spatial correlations are shared across time. Specifically, feature transformation is accomplished by transformation function \mathcal{T} . Here we set the function as a linear transformation function for clarity while other functions like a multi-layer perceptron can also be used. The function is defined as:

$$\mathbf{F}^s = \mathcal{T}(\mathbf{X}) = \mathbf{X} \mathbf{W}, \quad (5)$$

where $\mathbf{F}^s \in \mathbb{R}^{J \times T \times C'}$ is the high-level representations. After feature transformation, features are aggregated across time with aggregation function \mathcal{A}_t^s to obtain updated constrained feature \mathbf{C}^s . The whole process to obtain in constrained feature update is formulated as:

$$\mathbf{C}^s = \mathcal{A}_t^s(\mathbf{F}^s, \mathbf{A}^s) = [\mathbf{F}_{:,1}^s \mathbf{A}^s ||_t \cdots ||_t \mathbf{F}_{:,T}^s \mathbf{A}^s], \quad (6)$$

where $||_t$ is concatenation function along the time dimension. \mathbf{A}^s is vanilla spatial correlations and guide feature aggregation with the broadcast mechanism.

2) *Temporal-wise Feature Adjustment*: The temporal-wise feature adjustment is shown in the green part of Figure 2. Here temporal-specific spatial correlations $\mathbf{M}^s \in \mathbb{R}^{T \times J \times J}$ is inferred from the input sample to capture dynamic temporal-wise spatial correlations. Specifically, \mathbf{M}^s is extracted by the temporal-wise spatial correlation modeling function \mathcal{M}_t^s , which extract correlations between all pairs of joints. This function for a joint pair (j_p, j_q) is formulated as:

$$\mathbf{M}^s = \mathcal{M}_t^s(\mathbf{x}_p, \mathbf{x}_q) = \text{MLP}_1(\theta(\mathbf{x}_p) ||_s^p \phi(\mathbf{x}_q)), \quad (7)$$

where $(\mathbf{x}_p, \mathbf{x}_q)$ are from the input feature \mathbf{X} of the joint pair (j_p, j_q) and $||_s^p$ is pair-wise feature concatenation along the spatial dimension. θ and ϕ are two linear transformation functions, which project the joint features into low-dimensional representations to reduce computational cost. MLP_1 is a multi-layer perceptron, we utilize MLP because it can model complex spatial correlations. Note that \mathbf{M}^s is not required to be symmetric, this benefits correlation modeling by increasing analysis flexibility and enhancing representative ability. Besides, \mathbf{M}^s is also varied from different input samples.

Given the temporal-specific spatial correlations \mathbf{M}^s from input samples, we aggregate features with temporal-wise aggregation function \mathcal{A}_t^s , where aggregated feature $\hat{\mathbf{F}}^s \in \mathbb{R}^{J \times T \times C'}$ is obtained by:

$$\hat{\mathbf{F}}^s = \mathcal{A}_t^s(\mathbf{F}^s, \mathbf{M}^s) = [\mathbf{F}_{:,1}^s \mathbf{M}^s ||_t \cdots ||_t \mathbf{F}_{:,T}^s \mathbf{M}^s]. \quad (8)$$

Finally, the output representation with dynamic temporal-wise adjustment, $\mathbf{H}^{(l+1)}$, is obtained by adjusting constrained representation \mathbf{C}^s with temporal-specific representation $\hat{\mathbf{F}}^s$:

$$\mathbf{E}^s = \mathcal{U}_t^s(\mathbf{C}^s, \hat{\mathbf{F}}^s) = \mathbf{C}^s + \alpha \cdot \hat{\mathbf{F}}^s, \quad (9)$$

where α is a learnable parameter to control the adjustment intensity. Therefore, DS-GC can be formulated as:

$$\mathbf{Y} = \mathcal{U}^s(\mathcal{A}_c^s(\mathcal{T}(\mathbf{X}), \mathbf{A}^s), \mathcal{A}_t^s(\mathcal{T}(\mathbf{X}), \mathcal{M}_t^s(\mathbf{X}))). \quad (10)$$

Since DT-GC is spatiotemporal-equivalent to DS-GC, DT-GC can be directly obtained by replacing all operations in DS-GC with their spatiotemporal-equivalent counterparts.

3) *Discussion*: Compared with STS-GC/STD-GC, DSTD-GC contains three advantages: (1) *Parameter-saving*: STS-GC learn a spatial adjacency matrix \mathbf{A}^s and a temporal adjacency matrix \mathbf{A}^t , where the space complexity is $O(JT^2 + J^2T)$. Conversely, DSTD-GC saves a great many parameters by learning the previous two adjacency matrices in vanilla form with few extra operations, where the space complexity is $O(T^2 + J^2)$. As the joint number is always proportional to the sequence length, The space complexity for STS-GC is

$O(T^3)$ while the one DSTD-GC is only with $O(T^2)$. (2) *Joint optimization*: DSTD-GC learns shared graph correlations and dynamic correlation variations between different times or different joints. This mechanism has less optimization difficulty than learning optimal spatial correlation at different times or temporal correlations in different joints separately. (3) *Dynamic*: DSTD-GC adopts an adjustment strategy that can better model dynamic spatiotemporal correlations in different motion inputs.

C. Analysis of Graph Convolutions on Spatiotemporal Graphs

By reformulating several graph convolutions on spatiotemporal graphs into an uniform form, we assess their representation capabilities in human motion prediction. We begin by introducing the spatiotemporal graph decomposition constraint, and then evaluate several GCs on the basis of their spatial and temporal modeling capability. We focus exclusively on the correlation between distinct GCs, as correlation dominates feature aggregation and is hence critical for obtaining representative spatiotemporal feature. Based on previous formulation, we add (i) in the superscript to indicate different samples.

By comparing ST-GC (Equation 1) and STD-GC (Equation 4), the spatiotemporal correlations can be represented by a combination of spatial correlations and temporal correlations with the following constraints:

Constraint 1: $a_{(pm)(qn)}^{st(i)}$ equals to the product of $a_{npq}^{s(i)}$ and $a_{qmn}^{t(i)}$.

Note that here $a_{(pm)(qn)}^{st(i)}$ is the spatiotemporal correlation strength, $a_{npq}^{s(i)}$ is corresponding spatial correlation strength, and $a_{qmn}^{t(i)}$ is corresponding temporal correlation strength.

We further reformulate decomposed ST-GC from the spatial and temporal graph perspectives using the decomposition constraint. These two views can be defined as follows:

$$\begin{aligned} \mathbf{y}_{qn}^{(i)} &= \sum_p^J a_{npq}^{s(i)} \sum_m^T \mathbf{x}_{pm}^{(i)} (a_{qmn}^{t(i)} \mathbf{W}) \\ &= \sum_p^J a_{npq}^{s(i)} \sum_m^T \mathbf{x}_{pm}^{(i)} \mathbf{R}_{qmn}^{t(i)}, \end{aligned} \quad (11)$$

$$\begin{aligned} \mathbf{y}_{qn}^{(i)} &= \sum_m^T a_{qmn}^{t(i)} \sum_p^J \mathbf{x}_{pm}^{(i)} (a_{npq}^{s(i)} \mathbf{W}) \\ &= \sum_m^T a_{qmn}^{t(i)} \sum_p^J \mathbf{x}_{pm}^{(i)} \mathbf{R}_{npq}^{s(i)}, \end{aligned} \quad (12)$$

where $a_{npq}^{s(i)}$ and $a_{qmn}^{t(i)}$ are the spatial correlation weight and temporal correlation weight for the input sample. Furthermore, we combine correlation strength and feature transformation weights into a generalized weight matrix $\mathbf{R}_{npq}^{s(i)}$ or $\mathbf{R}_{qmn}^{t(i)}$. Therefore, the feature updating process consists of feature transformation with the generalized weight matrix and feature aggregation with temporal-wise spatial or spatial-wise temporal correlations. With these two formulations, we then analyze different graph GCs based on the spatial and temporal correlations for feature aggregation.

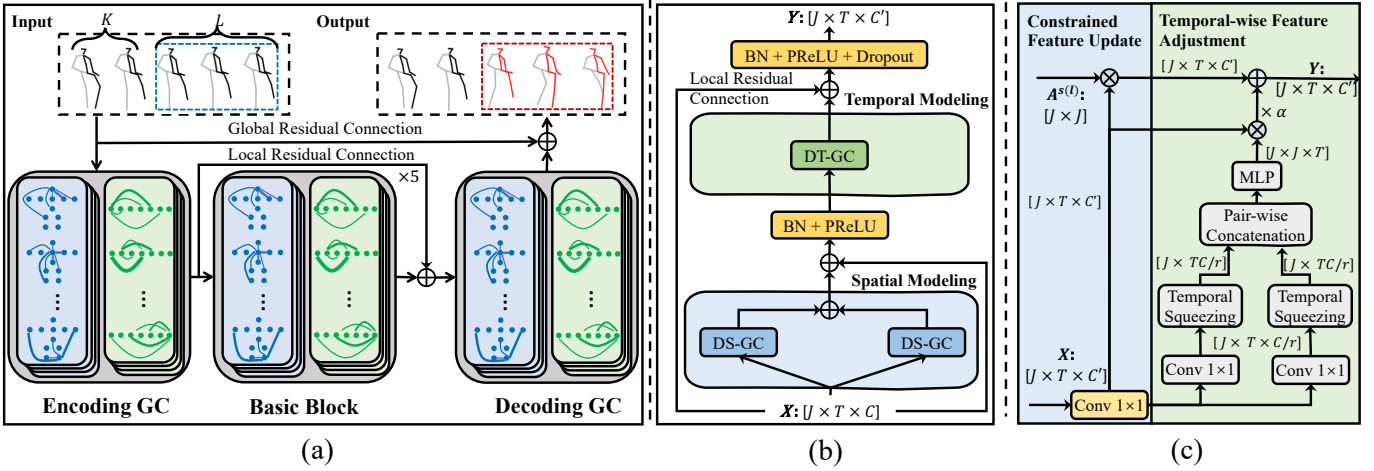


Fig. 3. (a) Problem reformulation and prediction framework. Human poses in the blue dashed box are duplicate inputs, while poses in the red box are target predictions. (b) The basic block of DSTD-GCN. The spatial modeling aims to adjust natural connection constraint and semantic connection constraint separately with two DS-GCs, while the temporal modeling refines self-loop temporal adjacency constraint with a DT-GC. (c) Implementation of DS-GC. Operations with different colors indicate different functions. The introduction of DT-GC is omitted due to the spatiotemporal-equivalence between DS-GC and DT-GC.

1) *Sample-shared Correlation-shared GCs*: Most recent works [25]–[27], [29], [38], [40] adopted correlation-shared GC, where joint vertices from all times share one spatial correlation and trajectory vertices for all joints share one temporal correlation. The whole GC process can be formulated as:

$$\mathbf{y}_{qn}^{(i)} = \sum_p^J \sum_m^T a_{pq}^s a_{mn}^t \mathbf{x}_{pm}^{(i)} \mathbf{W}, \quad (13)$$

$$\mathbf{y}_{qn}^{(i)} = \sum_p^J a_{pq}^s \sum_m^T \mathbf{x}_{pm}^{(i)} (a_{mn}^t \mathbf{W}), \quad (14)$$

$$\mathbf{y}_{qn}^{(i)} = \sum_m^T a_{mn}^t \sum_p^J \mathbf{x}_{pm}^{(i)} (a_{pq}^s \mathbf{W}). \quad (15)$$

Note that a_{pq}^s is temporal-shared spatial correlation strength and a_{mn}^t is spatial-shared spatial correlation strength, they are respectively from the vanilla form of the spatial and the temporal adjacency matrix \mathbf{A}^s and \mathbf{A}^t , respectively. Equation 14 and 15 are the reformulations of Equation 13 in spatial graph's view and temporal graph's view respectively. Besides, these two correlation strengths are stay unchanged across input samples. Therefore, the sample-shared correlation-shared GCs are subject to following constraints:

Constraint 2: $a_{m_1 p q}^{s(i)}$ and $a_{m_2 p q}^{s(i)}$ are forced to be the same, $a_{q_1 m n}^{t(i)}$ and $a_{q_2 m n}^{t(i)}$ are forced to be the same.

Constraint 3: $a_{m p q}^{s(i_1)}$ and $a_{m p q}^{s(i_2)}$ are forced to be the same, $a_{q m n}^{t(i_1)}$ and $a_{q m n}^{t(i_2)}$ are forced to be the same.

Note that i_1, i_2 are different input sample indices, m_1, m_2 are indices of different joints and q_1, q_2 indicate indices of different time.

2) *Sample-shared Correlation-unshared Graph GCs*: The only difference between sample-shared correlation-shared GCs and sample-shared correlation-unshared GCs is that the sample-shared spatiotemporal ones adopt unshared spatial

and temporal correlations. Sample-shared correlation-unshared GCs can be formulated as:

$$\mathbf{y}_{qn}^{(i)} = \sum_p^J \sum_m^T a_{npq}^s a_{qmn}^t \mathbf{x}_{pm}^{(i)} \mathbf{W}, \quad (16)$$

$$\mathbf{y}_{qn}^{(i)} = \sum_p^J a_{npq}^s \sum_m^T \mathbf{x}_{pm}^{(i)} (a_{qmn}^t \mathbf{W}), \quad (17)$$

$$\mathbf{y}_{qn}^{(i)} = \sum_m^T a_{qmn}^t \sum_p^J \mathbf{x}_{pm}^{(i)} (a_{npq}^s \mathbf{W}), \quad (18)$$

where a_{npq}^s is temporal-wise spatial correlation strength and a_{qmn}^t is spatial-shared temporal correlation strength. They are respectively from the spatial adjacency matrix and the temporal adjacency matrix. With the two unshared correlations, sample-shared correlation-unshared GCs capture evolving spatial relationships between joints at different action stages and diverse temporal relationships for different body parts. Thus, they generally outperform correlation-shared GCs. However, these correlations are optimized across all data and may not be optimized for individual action sequences. From the formula's view, sample-shared correlation-unshared GCs still suffer from *Constraint 2* but relax *Constraint 1* into the following constraint:

Constraint 4: $a_{m_1 p q}^{s(i)}$ and $a_{m_2 p q}^{s(i)}$ differ by a scaling factor, $a_{q_1 m n}^{t(i)}$ and $a_{q_2 m n}^{t(i)}$ differ by a scaling factor.

3) *Sample-specific Correlation-unshared Graph GCs*: In comparison to sample-shared correlation-unshared GCs, the dynamic ones infer sample-specific correlations between vertices and thus have a higher capacity for representation. The formulation for this GCs is:

$$\mathbf{y}_{qn}^{(i)} = \sum_p^J \sum_m^T a_{npq}^{s(i)} a_{qmn}^{t(i)} \mathbf{x}_{pm}^{(i)} \mathbf{W}, \quad (19)$$

$$\mathbf{y}_{qn}^{(i)} = \sum_p^J a_{npq}^{s(i)} \sum_m^T \mathbf{x}_{pm}^{(i)} (a_{qmn}^{t(i)} \mathbf{W}), \quad (20)$$

$$\mathbf{y}_{qn}^{(i)} = \sum_m^T a_{qmn}^{t(i)} \sum_p^J \mathbf{x}_{pm}^{(i)} (a_{npq}^{s(i)} \mathbf{W}). \quad (21)$$

Note that both $a_{npq}^{s(i)}$ and $a_{qmn}^{t(i)}$ are adjustable to the i -th input sample. Based on these formulations, sample-specific correlation-unshared GCs relax both *Constraint 2* and *3*. Concretely, they relax *Constraint 2* into Constraint 4 and relax *Constraint 3* into the following constraint:

Constraint 5: $a_{npq}^{s(i_1)}$ and $a_{npq}^{s(i_2)}$ differ by a scaling factor, $a_{qmn}^{t(i_1)}$ and $a_{qmn}^{t(i_2)}$ differ by a scaling factor.

We summarize different types of GCs on spatiotemporal graphs in Table I. It can be seen that sample-specific correlation-unshared GC is the least constrained spatiotemporal decompose GC. Our DSTD-GC belongs to sample-specific correlation-unshared GC. Thus, DSTD-GC has a stronger representation capability than previous graph convolutions [26], [31]. We can reformulate DSTD-GC into Equation 19, Equation 20 and Equation 21 respectively, as we will shown in the appendix.

D. Model Architecture

Based on DSTD-GC, we build a light-weight and powerful model DSTD-GCN, which builds upon the prediction framework proposed by [26]. We first introduce the prediction framework and then the implementation of DSTD-GCN.

1) *Prediction Framework:* We duplicate the last input human pose for L times and formulate a new input motion sequence $X_{1:K+L}$. Then the original prediction task is reformulated into predicting the residual motion sequence between $\tilde{X}_{1:K+L}$ and corresponding ground truth $X_{1:K+L}$. Based on the problem reformulation, the prediction framework is proposed as shown in Figure 3 (a). The framework contains a encoding GC layer to project motion input to high-level representation, several GC basic blocks for spatiotemporal representation modeling and a decoding GC to make predictions from motion feature. Besides, the global residual connection enforces the residual learning, while the local residual connection stabilizes the training process. The effectiveness of this framework is illustrated in recent studies [25], [26], [29]. With this framework, we can model the input and output human poses as a whole sequence and model associated spatiotemporal correlations, while the previous framework [28], [31] only models spatiotemporal correlations for the input frames. We will use this framework to build our model and compare different GCs.

2) *Model Implementation:* The entire network adopts the prediction framework and stacks five basic blocks. The basic block of DSTD-GCN is shown in Figure 3 (b), which contains two parallel DS-GCs for spatial modeling and a DT-GC for temporal modeling. Due to the spatiotemporal-equivalence between DS-GC and DS-GC, we only introduce the detailed implementation of DS-GC. Specifically, the modeling function \mathcal{M}_t^s receives inputs $X \in \mathbb{R}^{J \times C}$. We squeeze the temporal dimension into the channel dimension and direct extract

temporal-wise spatial correlations with a linear transformation. Since the computation for direct transformation from $T \times C$ to T is high. We utilize two linear transformation functions θ and ϕ to transform X into a neatly compact representation, then preforms a temporal squeeze operation. After, a pairwise concatenation and *MLP* are adapted to extract temporal-wise spatial correlations. The final result is a combination of constrained and dynamic correlations. We further consider prior knowledge connections and initialize constrained spatial correlations as natural connections and semantic connections such as relationships between two hands, respectively. The initial constrained temporal correlations are set as connections to oneself and its context frames.

IV. EXPERIMENTS

To evaluate the effectiveness of our proposed model, we run experiments on two standard benchmark motion capture datasets, which include Human3.6M [41] and the CMU Mocap dataset. Experiments are designed to answer the following research questions: (1) *what is the performance of DSTD-GC as compared to other GCs?* (2) *what is the performance of our proposed DSTD-GCN as compared to other state-of-art motion prediction methods?* (3) *what is the influence of different components and what insights and findings can we learn from the experimental results?*

A. Datasets Settings

1) *Human3.6M:* Human3.6M [41] is considered to be a wide-spread benchmark dataset for evaluating motion prediction. It contains 15 actions performed by 7 actors. Following the data preprocessing procedure of [11], [26], the original data in exponential mapping format is transformed into 3D joint coordinate space and a single pose is represented by 22 body joints. Besides, each data sequence is down-sampled to 25 FPS. The data from S5 and S11 are used as test and validation datasets, while the remaining 5 subjects are for training.

2) *CMU Mocap:* CMU Mocap dataset² is another well-known benchmark dataset. Each pose is represented by 25 body joints. The rest pre-processing procedure is the same as Human3.6M. We adopt the same train/test split strategy as [25], [26].

B. Comparison Settings

1) *Metrics:* The Mean Per Joint Position Error (MPJPE) is a standard evaluation metric used in previous studies [7], [11], [25]. With the predicted motion sequence $\tilde{X}_{K+1:K+L}$ and corresponding ground truth $X_{K+1:K+L}$, the MPJPE loss is defined as

$$\mathcal{L}_{\text{MPJPE}} = \frac{1}{J \times L} \sum_{t=K+1}^{K+L} \sum_{j=1}^J \|\tilde{p}_{j,t} - p_{j,t}\|_2, \quad (22)$$

where $\tilde{p}_{j,t} \in \mathbb{R}^D$ is the predicted j th joint position in frame t , while $p_{i,t} \in \mathbb{R}^D$ is the corresponding ground truth.

²<http://mocap.cs.cmu.edu/>

2) *Implementation Details*: We conduct all experiments on one RTX 3080 Ti GPU with the Pytorch framework [42]. For the comparison baseline and DSTD-GCN, we set the dropout rate as 0.1 and chose PReLU [43] as the activation function. Besides, all the models were trained with Adam optimizer [44] with an initial learning rate of $3e-3$, which decays by 0.9 for every 5 epochs. We also use MPJPE as the loss function and set the batch size as 32. For the test set and sequence length settings, we follow the experiment setting of Dang *et al.* [25]. We use the full test set and set the input length as 10, output length as 25.

TABLE I
COMPARISON OF DIFFERENT GRAPH CONVOLUTIONS.

GCs	Params.	Correlations Unshared Sample-specific	Constraints					MPJPE						
			1	2	3	4	5	80	160	320	400	560	1000	Average
ST	5.44M	-	-	-	-	-	-	8.70	16.16	31.34	39.16	53.91	85.30	39.09
VSTD	0.10M	✗	✗	✓	✓	✓	✓	8.48	16.38	33.63	42.33	58.37	93.05	42.04
FC [26]	0.29M	✗	✗	✓	✓	✓	✓	13.11	24.87	46.47	56.16	73.75	106.75	53.52
STS [31]	0.45M	✓	✗	✓	✓	✓	✓	8.33	15.62	30.97	38.77	53.70	85.34	38.79
TSD	0.46M	✓	✗	✓	✓	✓	✓	7.85	14.97	30.61	38.94	54.90	87.51	39.13
STD	0.46M	✓	✗	✓	✓	✓	✓	8.14	15.45	30.71	38.51	53.75	86.10	38.78
DTSD	0.13M	✓	✓	✓	✓	✓	✓	7.74	14.11	29.72	37.68	52.47	86.20	37.99
DSTD	0.13M	✓	✓	✓	✓	✓	✓	7.36	14.21	29.29	36.91	51.57	84.66	37.33

C. RQ1: Comparison with other GCs

we compare the parameters and prediction error of DSTD-GC against other GCs in Table I. Specifically, we exam three key aspects of DSTD-GCN: unshared correlation, sample-specific correlation, and stacking order invariance. For a fair comparison, we keep the prediction framework unchanged and merely replace graph convolution in the encoder, decoder and basic blocks. Moreover, we exchange linear transformation to a two-layer *MLP* for ST-GC, VST-GC, FC-TC and STS-GC. We also introduce TSD-GC and DTSD-GC by switching order of spatial and temporal GC in STD-GC and DSTD-GC, respectively. Besides, we initialized adjacency matrices randomly for all GCs.

1) *Shared Correlation vs Unshared Correlation*: As these two GCs are defined for decomposing spatiotemporal GC, we compare them with original ST-GC. We observe that correlation-shared GCs are more parameter-saving than correlation-unshared GCs but perform worse than ST-GC. On the other hand, the correlation-unshared GCs achieve similar errors as ST-GC, this suggests that unshared spatial and temporal correlations are more suitable forms for describing spatiotemporal correlations, because the unshared correlations can explicitly describe the varying spatiotemporal correlations in different body parts and different motion stages. Our DSTD-GC utilizes a shared correlation to store general correlation and a function to extract unshared correlation variances. Thus, our DSTD-GC is parameter-saving and explicitly models spatiotemporal correlations.

2) *Sample-shared Correlation vs Sample-specific Correlation*: We compare the two sample-shared GCs (TSD-GCD and STD-GC) with their sample-specific counterparts (DTSD-GC and DSTD-GC). We find sample-specific GC make consistent improvement in accuracy. The reason is that the learnt sample-shared correlation can't precisely depict correlations

in individual sequences, the correlation has to make a balance between various input samples. This global optimal strategy may introduce false correlation that disturb individual predictions. More studies about this is shown in Section IV-D3.

3) *Spatial-temporal Order vs Temporal-spatial Order*: As STD-GC and TSD-GC, DSTD-GC and DTSD-GC perform similarly, the modeling capability of spatiotemporal decomposed GC is invariant to the stacking order of spatial and temporal GCs.

D. RQ2: Comparison with the State-of-the-art

To evaluate the performance of DSTD-GCN, we present the quantitative and qualitative results on Human3.6M and CMU Mocap datasets. We first introduce the compared baselines and then DSTD-GCN's performance. Following literature from previous works [25], [26], we divide the results into short-term (< 500 msec) and long-term (> 500 msec) predictions.

1) *Baselines*: We select six state-of-the-art baselines, including RNN-based model (Residual sup [11]), CNN-based model (Traj-CNN [8]) and GCN-based model (FC-GCN [26], DMGNN [28] and MSR-GCN [25] and STS-GCN [31]). For GCN-based models, FC-GCN, DMGNN, and MSR-GCN belong to the sample-shared correlation-shared method, and STS-GCN³ is the only sample-shared correlation-unshared method. For the graph correlations, DMGNN adopts fixed correlations from body connections, while the other three GCN-based methods initialize the adjacency matrix randomly and then optimize it with back-propagation. Among all the baseline methods, FC-GCN, Traj-CNN, MSR-GCN, STS-GCN, and our approaches utilize the prediction framework depicted in Figure 3 (a).

2) *Results*: The detail quantitative comparisons for both short-term and long-term prediction results are presented in Table II and Table III. Besides, we also present the average results of selected frames in Table IV. Apparently, methods with the prediction framework make more accurate predictions with fewer parameters. Moreover, GCN-based methods generally outperform the RNN-based method (Residual Sup.) and CNN-based methods (Traj-CNN). For GCN-based methods, Correlation-unshared methods outperforms correlation-unshared methods in terms of prediction accuracy and parameter numbers. Note that MSR-GCN contains 65 GC layers and combines DCT temporal encoding [26] with multi-scale modeling, while STS-GCN and DSTD-GCN merely contain 7 GC layers with raw 3D inputs. With Constrained Dynamic Correlation Modeling, DSTD-GCN also models sample-specific correlations and achieves best prediction accuracy with fewest parameters. For qualitative comparison, we show two examples of the predicted poses for different methods in Figure 4. In the basketball scenario, correlation-shared methods generally work better than correlation-shared ones as correlation-unshared methods explicitly model individual joint's spatiotemporal correlations and thus can infer large movement from tiny motion cues. Here, both STS-GCN and our method capture the backward trend of the right feet. However, sample-shared modeling spatiotemporal correlations

³We utilized the model from RQ1

TABLE II

COMPARISONS OF PREDICTIONS ON HUMAN3.6M. THE BEST RESULTS ARE HIGHLIGHTED IN **BOLD**, WHILE THE SECOND BEST RESULTS ARE SHOWN IN UNDERLINE.

Action	Walking						Eating						Smoking						Discussion					
Millisecond	80	160	320	400	560	1000	80	160	320	400	560	1000	80	160	320	400	560	1000	80	160	320	400	560	1000
Residual sup. [11]	24.13	38.59	55.09	59.26	65.14	82.04	18.64	30.38	47.97	54.84	67.80	105.56	18.06	29.63	45.80	52.56	64.25	91.95	27.74	48.22	79.13	90.02	106.71	134.22
DMGNN [28]	15.52	27.42	46.20	54.96	58.86	83.74	10.34	19.84	37.60	46.66	57.95	86.55	9.94	18.90	35.03	42.82	53.23	77.76	14.77	30.86	62.05	75.26	93.24	123.67
FC-GCN [26]	12.29	23.03	39.77	46.12	54.05	59.75	8.36	16.90	33.19	40.70	53.39	77.75	7.94	16.24	31.90	38.90	50.74	72.62	12.50	27.40	58.51	71.68	91.61	121.53
Traj-CNN [8]	11.91	22.54	38.66	45.71	54.49	62.01	8.41	<u>16.56</u>	<u>32.44</u>	<u>39.82</u>	53.47	78.40	8.41	16.17	<u>31.06</u>	<u>37.58</u>	<u>49.30</u>	72.31	11.74	26.30	57.29	70.36	91.45	122.66
STS-GCN [31]	11.98	22.96	41.53	48.47	56.62	62.69	7.90	16.79	33.38	40.74	53.10	<u>76.73</u>	7.48	<u>15.69</u>	31.33	38.45	50.67	73.10	<u>11.39</u>	26.41	57.78	71.08	91.16	120.79
MSR-GCN [25]	12.16	22.65	38.64	<u>45.24</u>	52.72	63.04	8.39	17.05	33.03	40.43	52.54	77.11	8.02	16.27	31.32	38.15	49.45	71.64	11.98	26.76	<u>57.08</u>	69.74	88.59	117.59
Ours	11.05	22.35	<u>38.81</u>	45.19	52.70	<u>59.76</u>	6.95	15.51	31.74	39.19	51.86	76.19	6.64	14.75	29.78	36.67	48.09	71.16	9.98	24.37	54.53	67.40	87.00	116.30
Action	Directions						Greetings						Phoning						Posing					
Millisecond	80	160	320	400	560	1000	80	160	320	400	560	1000	80	160	320	400	560	1000	80	160	320	400	560	1000
Residual sup. [11]	21.93	37.38	61.51	71.86	88.09	122.08	35.28	61.98	99.06	111.04	127.44	160.59	21.05	35.49	57.89	67.26	83.74	130.34	32.99	59.71	104.87	123.67	158.74	300.18
DMGNN [28]	10.77	22.81	46.70	57.35	73.51	104.37	20.45	41.13	78.99	94.34	114.68	148.75	12.35	24.25	47.22	58.27	73.62	113.05	15.40	32.07	67.36	84.19	113.60	171.56
FC-GCN [26]	8.97	19.87	43.35	53.74	71.01	101.79	18.65	38.68	77.74	93.39	114.43	148.69	10.24	21.02	42.54	52.30	69.56	104.50	13.66	29.89	66.62	84.05	113.56	171.31
Traj-CNN [8]	8.69	19.29	43.57	54.36	74.56	109.42	15.81	35.12	73.56	<u>88.89</u>	<u>110.78</u>	149.55	10.14	20.52	41.95	51.86	69.29	104.41	12.09	26.94	<u>62.44</u>	<u>79.33</u>	<u>108.36</u>	170.86
STS-GCN [31]	<u>7.82</u>	<u>18.72</u>	<u>42.58</u>	53.25	70.95	102.10	<u>15.33</u>	<u>35.01</u>	<u>73.44</u>	89.08	12.19	<u>143.91</u>	9.54	20.35	41.55	<u>51.07</u>	68.32	103.69	11.61	27.60	63.85	81.23	111.68	168.41
MSR-GCN [25]	8.61	19.65	43.28	53.82	71.18	<u>100.59</u>	16.48	36.95	77.32	93.38	116.26	147.26	10.10	20.74	<u>41.51</u>	51.26	68.29	104.27	12.79	29.38	66.95	85.01	116.27	174.33
Ours	6.86	17.39	40.96	51.67	69.05	99.05	14.27	33.53	72.15	87.31	108.66	142.28	8.52	19.22	40.31	49.87	66.69	102.20	10.08	25.40	60.60	77.34	106.54	163.31
Action	Purchases						Sitting						Sitting Down						Taking Photo					
Millisecond	80	160	320	400	560	1000	80	160	320	400	560	1000	80	160	320	400	560	1000	80	160	320	400	560	1000
Residual sup. [11]	30.54	52.89	86.31	99.07	121.00	169.66	22.08	38.58	64.59	75.94	96.33	145.90	27.73	47.24	79.55	93.33	117.92	170.19	21.53	37.30	63.83	75.78	95.70	145.82
DMGNN [28]	17.60	36.24	69.43	83.20	104.09	145.26	11.77	23.42	48.33	60.69	80.75	123.31	16.93	32.04	62.19	76.52	101.16	153.00	11.49	23.07	46.89	58.46	78.20	121.69
FC-GCN [26]	15.60	32.78	<u>65.72</u>	<u>79.25</u>	<u>100.19</u>	141.14	10.62	21.90	46.33	57.91	79.38	122.44	16.14	31.12	61.74	76.46	99.24	149.30	9.88	20.89	44.95	56.58	76.52	119.33
Traj-CNN [8]	14.54	31.88	66.55	80.75	103.65	141.01	10.97	21.17	45.48	57.50	78.95	120.12	16.13	29.56	58.74	72.59	97.00	146.96	10.43	20.64	44.37	55.83	76.78	120.11
STS-GCN [31]	<u>13.87</u>	31.66	66.00	80.04	102.46	142.46	<u>9.63</u>	<u>20.65</u>	<u>45.22</u>	<u>57.26</u>	78.96	122.03	14.98	29.60	59.94	73.55	98.80	149.52	9.15	19.87	<u>43.42</u>	54.99	76.15	118.76
MSR-GCN [25]	14.75	32.39	66.13	79.64	101.63	<u>139.16</u>	10.53	21.99	46.26	57.80	78.20	<u>120.04</u>	16.10	31.63	62.45	76.84	102.84	155.47	9.89	21.01	44.56	56.30	77.97	121.91
Ours	12.68	29.65	62.29	75.79	97.54	137.76	8.78	19.32	42.88	54.33	74.94	117.75	14.10	28.03	57.33	71.18	96.08	<u>147.25</u>	8.41	18.84	42.00	53.50	74.50	117.91
Action	Waiting						Walking Dog						Walking Together						Average					
Millisecond	80	160	320	400	560	1000	80	160	320	400	560	1000	80	160	320	400	560	1000	80	160	320	400	560	1000
Residual sup. [11]	25.78	44.52	72.29	82.44	98.79	136.76	39.19	67.36	105.56	117.96	135.99	186.09	22.03	36.08	54.91	60.30	67.89	85.19	25.91	44.36	71.86	82.35	99.90	144.44
DMGNN [28]	12.89	25.70	51.27	62.84	79.82	112.99	26.09	50.47	88.90	102.55	118.44	156.09	13.76	25.55	44.49	53.47	59.41	79.06	14.67	28.91	55.51	67.44	84.04	129.06
FC-GCN [26]	11.43	23.99	50.06	61.48	78.15	108.77	23.39	46.17	83.47	95.96	<u>110.98</u>	146.24	10.47	21.04	38.47	45.19	54.71	66.96	12.68	26.06	52.29	63.58	81.17	114.14
Traj-CNN [8]	10.51	21.76	45.79	56.29	73.36	104.53	21.30	43.29	80.77	94.50	<u>115.56</u>	153.50	10.30	21.11	38.48	44.82	54.78	68.00	12.09	24.86	50.74	61.95	80.78	114.92
STS-GCN [31]	<u>10.00</u>	21.93	46.98	58.22	76.39	107.68	20.79	43.56	81.81	95.20	114.36	151.92	<u>10.06</u>	<u>20.69</u>	39.07	46.00	54.92	<u>62.91</u>	11.43	24.77	<u>51.16</u>	<u>62.58</u>	81.12	113.78
MSR-GCN [25]	10.68	23.06	48.25	59.23	76.33	106.27	20.65	42.88	80.35	<u>93.31</u>	111.89	148.24	10.56	20.92	<u>37.40</u>	<u>43.85</u>	52.94	65.94	12.11	25.56	51.64	62.93	81.14	114.19
Ours	8.71	20.15	44.28	55.25	73.19	105.66	19.64	41.82	77.61	90.24	109.84	<u>147.68</u>	9.07	19.79	36.33	42.67	50.54	61.22	10.38	23.34	48.77	59.84	77.81	111.02

TABLE III

COMPARISONS OF PREDICTION RESULTS ON CMU MOCAP DATASET. THE BEST RESULTS ARE HIGHLIGHTED IN **BOLD**, WHILE THE SECOND BEST RESULTS ARE SHOWN IN UNDERLINE.

Action	Basketball						Basketball Signal						Directing Traffic						Jumping					
Millisecond	80	160	320	400	560	1000	80	160	320	400	560	1000	80	160										

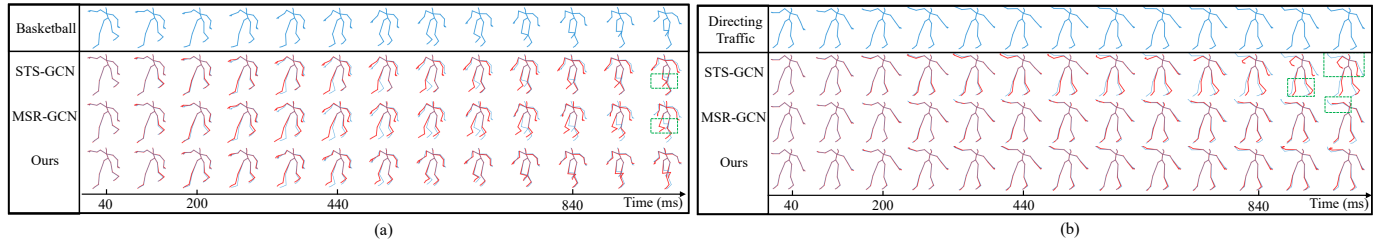


Fig. 4. Visualization of predicted results of state-of-the-art methods on two action examples on CMU-Mocap dataset. The blue and red poses indicate ground truths and predictions respectively. (a) Basketball. (b) Directing Traffic.

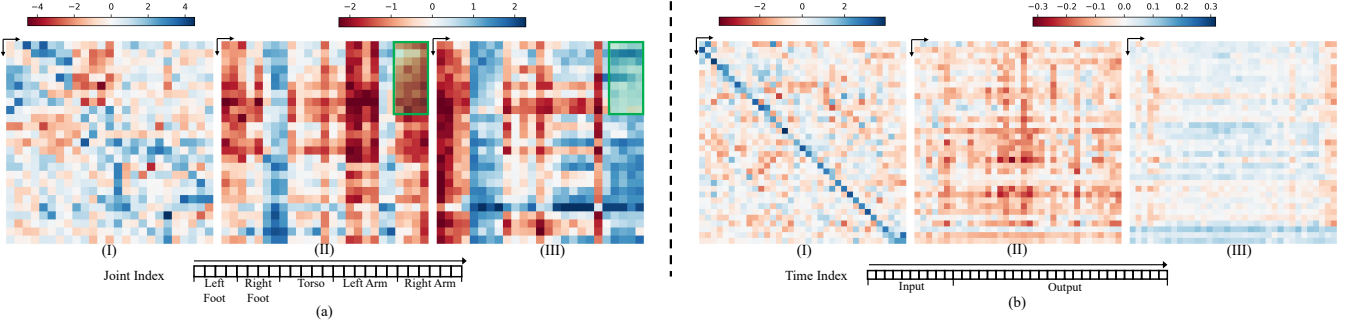


Fig. 5. Visualization of spatial and temporal correlation. Color brightness indicates correlation strength. (a) Spatial correlation from a predicted human pose frame. (b) Temporal correlation from a joint trajectory. (I) Constrained correlation. (II) and (III) are sample-specific correlation adjustments of a pose frame or a joint trajectory for two different action sequences.

make more accurate predictions under different scenarios.

3) *Visualization of Constrained Dynamic Correlations*: To better understand why our method takes effect, we visualize the sample spatial and temporal correlations from the two visualization sequences in Figure 5. We obtain two observations: (1) The constrained correlation strength is larger than the adjusted one, demonstrating that the basics of motion prediction come from shared constrained correlation. (2) Sample-specific correlation adaptively extracts adjustments which contribute to accurate motion prediction. As shown in Figure 5 (a) (II) and (III), the adjustment strength from the right arm to the feet (green box) is enhanced in basketball and reduced in directing traffic. These adjustments are reasonable because arms and feet collaborate intensively in the basketball example but feet are still and unrelated to the movement of the right arm in the directing traffic case. Moreover, we also present temporal correlation adjustments from a right foot joint in Figure 5 (b), we find the adjustment strengths are generally stronger in the basketball case. As the right foot moves backward in the basketball example, it correlates to other vertices of the trajectory more intensively. With this visualization, we observe that our proposed Constrained Dynamic Correlation Modeling can generate sample-specific correlation and thus make more accurate predictions.

4) *Effectiveness Analysis*: We present model parameters and inference time of single epoch in Table IV. Generally, correlation-unshared methods outperform other methods in prediction accuracy and parameters. Our method outperforms other methods in prediction accuracy with fewest parameters. The parameter number of our method is half of the most lightweight model STS-GCN and only 3% of the best baseline

MSR-GCN on the CMU Mocap dataset. Besides, our method is slightly slower than STS-GCN due to the additional computation of unshared correlation adjustments.

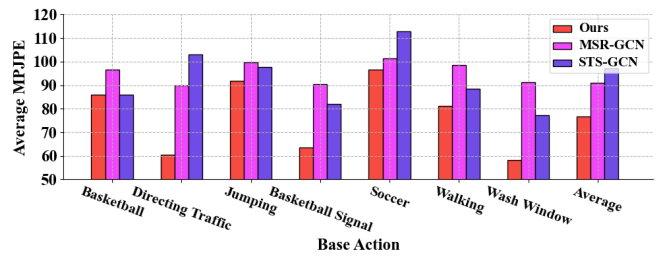


Fig. 6. Comparison of Unseen Action Prediction. On each of the seven actions in the CMU Mocap dataset, we train STS-GCN [31], MSR-GCN [25], and our model. Then, we test these models on all actions. Our method outperforms STS-GCN and MSR-GCN with lower MPJPE.

TABLE IV
COMPARISON SUMMARY OF AVERAGE MPJPE, PARAMETER NUMBERS
AND INFERENCE TIME PER EPOCH

Model	Human3.6M			CMU Mocap		
	MPJPE	Params.	Inference	MPJPE	Params.	Inference
DMGNN [28]	63.27	46.90M	422ms	50.84	46.94M	590ms
FC-GCN [26]	58.32	2.55M	46ms	40.30	2.70M	47ms
Traj-CNN [8]	57.56	1.20M	95ms	38.62	1.20M	110ms
STS-GCN [31]	57.47	0.40M	39ms	38.64	0.46M	41ms
MSR-GCN [25]	57.88	6.30M	70ms	38.10	6.37M	82ms
Ours	55.19	0.18M	48ms	35.93	0.20M	50ms

TABLE V
COMPARISON OF ABLATION VARIANTS

Model	MPJPE					
	80	160	320	400	560	1000
DSTD-C	7.84	15.02	30.81	38.90	54.26	88.74
DSTD-D	10.68	19.34	35.69	43.53	57.56	89.81
DSTD-R	8.62	16.37	33.15	41.90	58.55	90.69
DSTD-P	7.58	14.25	29.02	36.73	51.35	81.81
DSTD-F	7.99	14.97	30.23	37.53	52.96	84.23
DSTD-S	8.89	16.24	32.48	40.87	56.85	91.38
DSTD-T	7.68	15.07	31.47	39.78	55.13	87.14
DSTD	7.33	13.90	28.37	35.91	50.11	79.95
	Average					

E. RQ3: Ablation Study

We investigate some major components of our method in this section by comparing DSTD-GCN to its variants and other state-of-the-art methods. We propose eight ablation variants: (1) DSTD-C: DSTD-GCN only with constrained correlation update in DG-GC and DT-GC; (2) DSTD-D: DSTD-GCN only with dynamic correlation adjustments in DG-GC and DT-GC. (3) DSTD-R: constrained correlation is used to update dynamic correlation adjustments. (4) DSTD-P: DSTD-GCN without any predefined correlations. (6) DSTD-F: replacing DS-GCs and DT-GCs by S-GCs and T-GCs, respectively. (7) DSTD-S: replacing DT-GCs by DS-GCs. (8) DSTD-T: all DS-GCs are replaced by DT-GCs. The detail results are shown in Table V.

1) *Constrained Dynamic Correlation Modeling*: We investigate our proposed constrained dynamic modeling strategy by comparing DSTD-C, DSTD-D, DSTD-R and DSTD. First, we study the relationships between the constrained correlation and the dynamic correlation. Comparing the prediction error of DSTD-C and DSTD-D: we observe that DSTD-C outperforms DSTD-D by 3.51, indicating that constrained correlations are more important for accurate motion prediction. Then, we study the updating strategy studying DSTD-R. DSTD-R performs worse than DSTD by 5.64, indicating that constrained correlation adjustment disturbs dynamic correlation. So dynamic correlations adjust constrained correlations but not vice versa.

2) *Prior Connections*: We study the effects of prior connections in constrained correlations with DSTD-F, DSTD-P and DSTD. Comparing the improvement in average MPJPE for prior connection (DSTD-P and DSTD) and Constrained Dynamic Correlation Modeling (DSTD-F and DSTD), we find the reduction of prior connections (0.86) is much less than the reduction of Constrained Dynamic Correlation Modeling (2.06). Note that other state-of-the-art baselines don't get prior connections, DSTD-P still outperforms the best baseline MSR-GCN by 1.31 in average MPJPE, indicating the effectiveness of our proposed Constrained Dynamic Correlation Modeling.

3) *Spatial and Temporal GCs*: To investigate the contribution of spatial and temporal GCs, we compare DSTD-S, DSTD-T, and DSTD. We observe that (1) DSTD outperforms DSTD-S and DSTD-T by 13.98 and 11.68, respectively, indicating that individual spatial or temporal GCs cannot make accurate prediction results and emphasizing the importance of spatiotemporal correlation modeling; and (2) DSTD-T outperforms DSTD-S by 2.30, demonstrating that temporal

correlations are more important than spatial correlations for human motion prediction.

4) *Unseen Action Prediction*: To further understand the effectiveness of our proposed model, we conduct experiments on unseen action predictions. Specifically, we train the model on one action and test on all actions. Figure 6 shows the comparison results. Our method outperforms two state-of-the-art models by a large margin. It illustrates that our DSTD-GCN is capable of generating sample-specific spatiotemporal correlations that may be used to improve human motion prediction in response to the individualized motions associated with various actions.

F. Limitations

We only design a multi-layer perceptron based on pair-wise concatenation to extract temporal/spatial-wise spatial/temporal correlation adjustments. This exhaustive correlation modeling strategy calculates correlations between some unrelated vertices. There is space to design a more powerful and efficient correlation modeling strategy. Another limitation is the accuracy of unseen action prediction. The unseen action prediction error is 76.85, while the supervised prediction error is 35.93. There is space to explore methods for unseen action predictions. One possible method is to combine constrained dynamic modeling with few-shot learning [45].

V. CONCLUSIONS

In this work, we propose a novel Dynamic SpatioTemporal Decompose Graph Convolutions (DSTD-GC) for human motion prediction. DSTD-GC deploys the Constrained Dynamic Correlation Modeling, which extends conventional graph convolutions by combining constrained correlations from training or prior knowledge and dynamic correlations from input motion sequences. We make mathematical analysis and conduct extensive experiments to illustrate the power spatiotemporal modeling capability of DSTD-GC, which break certain constraints of state-of-the-art graph convolutions on spatiotemporal graphs. With this strategy, we propose DSTD-GCN which outperforms other state-of-the-art methods in prediction accuracy with the fewest parameters.

ACKNOWLEDGMENTS

This work was supported partly by the National Natural Science Foundation of China (Grant No. 62173045, 61673192), and partly by the Fundamental Research Funds for the Central Universities (Grant No. 2020XD-A04-2).

APPENDIX

FORMULA DERIVATION FROM DSTD-GC TO DYNAMIC CORRELATION-UNSHARED METHOD.

We give the derivation from feature updating process of DSTD-GC to Equation 19, 20 and 21, respectively. First, we rewrite feature updating of DS-GC for joint q of time n :

$$\mathbf{y}_{qn}^{s(i)} = \sum_p^J r_{npq}^{s(i)} \mathbf{x}_{pn}^{(i)} \mathbf{W}_1, \quad (23)$$

where $r_{npq}^{s(i)}$ is from $\mathbf{R}^{s(i)}$ and $\mathbf{R}^{s(i)} = \mathbf{A}^s + \mathbf{M}^{s(i)}$. Recall that \mathbf{A}^s is temporal-shared constrained spatial correlation and $\mathbf{M}^{s(i)}$ is from Equation 7, we add i to highlight sample-specific adjustments. According to the spatiotemporal-equivalence between DS-GC and DT-GC. The feature updating of DT-GC can be formulated as:

$$\mathbf{y}_{qn}^{t(i)} = \sum_m^T r_{qmn}^{t(i)} \mathbf{x}_{qm}^{(i)} \mathbf{W}_2. \quad (24)$$

By alternatively apply Equation 23 and 24, DSTD-GC can be formulated as:

$$\mathbf{y}_{qn}^{st(i)} = \sum_p^J \sum_m^T r_{npq}^{s(i)} r_{qmn}^{t(i)} \mathbf{x}_{pm}^{(i)} \mathbf{W}, \quad (25)$$

where $\mathbf{W} = \mathbf{W}_1 \mathbf{W}_2$. It can be seen that Equation 19 is the same as Equation 25 since $r_{npq}^{s(i)}$ is equivalent to $a_{npq}^{s(i)}$ and $r_{qmn}^{t(i)}$ is equivalent to $a_{qmn}^{t(i)}$. Similarly, Equation 25 can be reformulated as follows:

$$\mathbf{y}_{qn}^{st(i)} = \sum_p^J r_{npq}^{s(i)} \sum_m^T \mathbf{x}_{pm}^{(i)} (r_{qmn}^{t(i)} \mathbf{W}), \quad (26)$$

$$\mathbf{y}_{qn}^{st(i)} = \sum_m^T r_{qmn}^{t(i)} \sum_p^J \mathbf{x}_{pm}^{(i)} (r_{npq}^{s(i)} \mathbf{W}). \quad (27)$$

It can be seen that Equation 20 is the same as Equation 26 and Equation 21 is the same as Equation 27.

REFERENCES

- [1] B. Paden, M. Čáp, S. Z. Yong, D. Yershov, and E. Frazzoli, “A survey of motion planning and control techniques for self-driving urban vehicles,” *IEEE Transactions on intelligent vehicles*, vol. 1, no. 1, pp. 33–55, 2016.
- [2] Y. Kong and Y. Fu, “Human action recognition and prediction: A survey,” *arXiv preprint arXiv:1806.11230*, 2018.
- [3] V. V. Unhelkar, P. A. Lasota, Q. Tyroller, R.-D. Buhai, L. Marceau, B. Deml, and J. A. Shah, “Human-aware robotic assistant for collaborative assembly: Integrating human motion prediction with planning in time,” *IEEE Robotics and Automation Letters*, vol. 3, no. 3, pp. 2394–2401, 2018.
- [4] N. F. Troje, “Decomposing biological motion: A framework for analysis and synthesis of human gait patterns,” *Journal of vision*, vol. 2, no. 5, pp. 2–2, 2002.
- [5] G. W. Taylor, L. Sigal, D. J. Fleet, and G. E. Hinton, “Dynamical binary latent variable models for 3d human pose tracking,” in *2010 IEEE Computer Society Conference on Computer Vision and Pattern Recognition*. IEEE, 2010, pp. 631–638.
- [6] A. M. Lehrmann, P. V. Gehler, and S. Nowozin, “Efficient nonlinear markov models for human motion,” in *Proceedings of the IEEE Conference on Computer Vision and Pattern Recognition*, 2014, pp. 1314–1321.
- [7] C. Li, Z. Zhang, W. S. Lee, and G. H. Lee, “Convolutional sequence to sequence model for human dynamics,” in *Proceedings of the IEEE Conference on Computer Vision and Pattern Recognition*, 2018, pp. 5226–5234.
- [8] X. Liu, J. Yin, J. Liu, P. Ding, J. Liu, and H. Liu, “Trajectorycnn: a new spatio-temporal feature learning network for human motion prediction,” *IEEE Transactions on Circuits and Systems for Video Technology*, vol. 31, no. 6, pp. 2133–2146, 2020.
- [9] A. F. Al-aqel and M. A. Khan, “Attention mechanism for human motion prediction,” in *2020 3rd International Conference on Computer Applications & Information Security (ICCAIS)*. IEEE, 2020, pp. 1–6.
- [10] X. Guo and J. Choi, “Human motion prediction via learning local structure representations and temporal dependencies,” in *Proceedings of the AAAI Conference on Artificial Intelligence*, vol. 33, no. 01, 2019, pp. 2580–2587.
- [11] J. Martinez, M. J. Black, and J. Romero, “On human motion prediction using recurrent neural networks,” in *Proceedings of the IEEE conference on computer vision and pattern recognition*, 2017, pp. 2891–2900.
- [12] K. Fragkiadaki, S. Levine, P. Felsen, and J. Malik, “Recurrent network models for human dynamics,” in *Proceedings of the IEEE international conference on computer vision*, 2015, pp. 4346–4354.
- [13] Y. Tang, L. Ma, W. Liu, and W. Zheng, “Long-term human motion prediction by modeling motion context and enhancing motion dynamic,” *arXiv preprint arXiv:1805.02513*, 2018.
- [14] Z. Liu, S. Wu, S. Jin, Q. Liu, S. Lu, R. Zimmermann, and L. Cheng, “Towards natural and accurate future motion prediction of humans and animals,” in *Proceedings of the IEEE/CVF Conference on Computer Vision and Pattern Recognition*, 2019, pp. 10 004–10 012.
- [15] D. Pavllo, C. Feichtenhofer, M. Auli, and D. Grangier, “Modeling human motion with quaternion-based neural networks,” *International Journal of Computer Vision*, vol. 128, no. 4, pp. 855–872, 2020.
- [16] X. Shu, L. Zhang, G.-J. Qi, W. Liu, and J. Tang, “Spatiotemporal co-attention recurrent neural networks for human-skeleton motion prediction,” *IEEE Transactions on Pattern Analysis and Machine Intelligence*, 2021.
- [17] H. Wang, J. Dong, B. Cheng, and J. Feng, “Pvred: A position-velocity recurrent encoder-decoder for human motion prediction,” *IEEE Transactions on Image Processing*, vol. 30, pp. 6096–6106, 2021.
- [18] L.-Y. Gui, Y.-X. Wang, X. Liang, and J. M. Moura, “Adversarial geometry-aware human motion prediction,” in *Proceedings of the European Conference on Computer Vision (ECCV)*, 2018, pp. 786–803.
- [19] A. Hernandez, J. Gall, and F. Moreno-Noguer, “Human motion prediction via spatio-temporal inpainting,” in *Proceedings of the IEEE/CVF International Conference on Computer Vision*, 2019, pp. 7134–7143.
- [20] Q. Cui, H. Sun, Y. Kong, X. Zhang, and Y. Li, “Efficient human motion prediction using temporal convolutional generative adversarial network,” *Information Sciences*, vol. 545, pp. 427–447, 2021.
- [21] Q. Ke, M. Bennamoun, H. Rahmani, S. An, F. Sohel, and F. Boussaid, “Learning latent global network for skeleton-based action prediction,” *IEEE Transactions on Image Processing*, vol. 29, pp. 959–970, 2019.
- [22] J. N. Kundu, M. Gor, and R. V. Babu, “Bihmp-gan: Bidirectional 3d human motion prediction gan,” in *Proceedings of the AAAI conference on artificial intelligence*, vol. 33, no. 01, 2019, pp. 8553–8560.
- [23] Y. Cai, L. Huang, Y. Wang, T.-J. Cham, J. Cai, J. Yuan, J. Liu, X. Yang, Y. Zhu, X. Shen *et al.*, “Learning progressive joint propagation for human motion prediction,” in *European Conference on Computer Vision*. Springer, 2020, pp. 226–242.
- [24] E. Aksan, M. Kaufmann, P. Cao, and O. Hilliges, “A spatio-temporal transformer for 3d human motion prediction,” in *2021 International Conference on 3D Vision (3DV)*. IEEE, 2021, pp. 565–574.
- [25] L. Dang, Y. Nie, C. Long, Q. Zhang, and G. Li, “Msr-gen: Multi-scale residual graph convolution networks for human motion prediction,” in *Proceedings of the IEEE/CVF International Conference on Computer Vision*, 2021, pp. 11 467–11 476.
- [26] W. Mao, M. Liu, M. Salzmann, and H. Li, “Learning trajectory dependencies for human motion prediction,” in *Proceedings of the IEEE/CVF International Conference on Computer Vision*, 2019, pp. 9489–9497.
- [27] W. Mao, M. Liu, and M. Salzmann, “History repeats itself: Human motion prediction via motion attention,” in *European Conference on Computer Vision*. Springer, 2020, pp. 474–489.
- [28] M. Li, S. Chen, Y. Zhao, Y. Zhang, Y. Wang, and Q. Tian, “Dynamic multiscale graph neural networks for 3d skeleton based human motion prediction,” in *Proceedings of the IEEE/CVF Conference on Computer Vision and Pattern Recognition*, 2020, pp. 214–223.
- [29] Q. Cui, H. Sun, and F. Yang, “Learning dynamic relationships for 3d human motion prediction,” in *Proceedings of the IEEE/CVF conference on computer vision and pattern recognition*, 2020, pp. 6519–6527.
- [30] Z. Liu, P. Su, S. Wu, X. Shen, H. Chen, Y. Hao, and M. Wang, “Motion prediction using trajectory cues,” in *Proceedings of the IEEE/CVF International Conference on Computer Vision*, 2021, pp. 13 299–13 308.
- [31] T. Sofianos, A. Sampieri, L. Franco, and F. Galasso, “Space-time-separable graph convolutional network for pose forecasting,” in *Proceedings of the IEEE/CVF International Conference on Computer Vision*, 2021, pp. 11 209–11 218.
- [32] P. Su, Z. Liu, S. Wu, L. Zhu, Y. Yin, and X. Shen, “Motion prediction via joint dependency modeling in phase space,” in *Proceedings of the 29th ACM International Conference on Multimedia*, 2021, pp. 713–721.
- [33] Z. Liu, K. Lyu, S. Wu, H. Chen, Y. Hao, and S. Ji, “Aggregated multi-gans for controlled 3d human motion prediction,” in *Proceedings of the AAAI Conference on Artificial Intelligence*, vol. 35, no. 3, 2021, pp. 2225–2232.
- [34] K. Lyu, Z. Liu, S. Wu, H. Chen, X. Zhang, and Y. Yin, “Learning human motion prediction via stochastic differential equations,” in *Proceedings of the 29th ACM International Conference on Multimedia*, 2021, pp. 4976–4984.

- [35] T. Derr, Y. Ma, and J. Tang, "Signed graph convolutional networks," in *2018 IEEE International Conference on Data Mining (ICDM)*. IEEE, 2018, pp. 929–934.
- [36] G. Qian, A. Abualshour, G. Li, A. Thabet, and B. Ghanem, "Pugen: Point cloud upsampling using graph convolutional networks," in *Proceedings of the IEEE/CVF Conference on Computer Vision and Pattern Recognition*, 2021, pp. 11683–11692.
- [37] B. Yu, H. Yin, and Z. Zhu, "Spatio-temporal graph convolutional networks: A deep learning framework for traffic forecasting," *arXiv preprint arXiv:1709.04875*, 2017.
- [38] M. Li, S. Chen, Y. Zhao, Y. Zhang, Y. Wang, and Q. Tian, "Multiscale spatio-temporal graph neural networks for 3d skeleton-based motion prediction," *IEEE Transactions on Image Processing*, vol. 30, pp. 7760–7775, 2021.
- [39] T. N. Kipf and M. Welling, "Semi-supervised classification with graph convolutional networks," *arXiv preprint arXiv:1609.02907*, 2016.
- [40] S. Yan, Y. Xiong, and D. Lin, "Spatial temporal graph convolutional networks for skeleton-based action recognition," in *Thirty-second AAAI conference on artificial intelligence*, 2018.
- [41] C. Ionescu, D. Papava, V. Olaru, and C. Sminchisescu, "Human3. 6m: Large scale datasets and predictive methods for 3d human sensing in natural environments," *IEEE transactions on pattern analysis and machine intelligence*, vol. 36, no. 7, pp. 1325–1339, 2013.
- [42] A. Paszke, S. Gross, F. Massa, A. Lerer, J. Bradbury, G. Chanan, T. Killeen, Z. Lin, N. Gimelshein, L. Antiga *et al.*, "Pytorch: An imperative style, high-performance deep learning library," *Advances in neural information processing systems*, vol. 32, 2019.
- [43] K. He, X. Zhang, S. Ren, and J. Sun, "Delving deep into rectifiers: Surpassing human-level performance on imagenet classification," in *Proceedings of the IEEE international conference on computer vision*, 2015, pp. 1026–1034.
- [44] D. P. Kingma and J. Ba, "Adam: A method for stochastic optimization," *arXiv preprint arXiv:1412.6980*, 2014.
- [45] L.-Y. Gui, Y.-X. Wang, D. Ramanan, and J. M. Moura, "Few-shot human motion prediction via meta-learning," in *Proceedings of the European Conference on Computer Vision (ECCV)*, 2018, pp. 432–450.